6th IAHR International Meeting of the Workgroup on Cavitation and Dynamic Problems in Hydraulic Machinery and Systems, September 9-11, 2015, Ljubljana, Slovenia

NUMERICAL ANALYSIS OF WATER ELEVATION IN A HYDROPOWER PLANT SURGE TANK

Muris Torlak[1,*], **Adis Bubalo**[2], **Ejub Džaferović**[1]

[1] University of Sarajevo - Mechanical Engineering Faculty
Vilsonovo šetalište 9, 71000 Sarajevo, Bosnia-Herzegovina
[2] Elektroprivreda BiH - Hidroelektrane na Neretvi
Jaroslava Černija br.1, 88420 Jablanica, Bosnia-Herzegovina
* corresponding author, corresponding e-mail address: torlak@mef.unsa.ba

Abstract

Water elevation in a surge tank during closure of the turbine wicket gates in a hydropower plant is calculated using a computational fluid dynamics (CFD) method with a free-surface model based on volume-of-fluid approach. Stagnation condition is applied at the inlet boundary after a proper initialization. The results are compared with the experimental data from the real-scale test and with a simple analytical solution. CFD prediction of the water level agrees considerably well with the meassured values, while the analytical solution exhibits strong over-prediction of the oscillation amplitudes. Thus, present CFD calculations provide a reliable approach to assess surge tank perfromance which should ensure water surface motion within acceptable limits and proper pressure damping. In the further work, the CFD results will be used to improve the surge-tank model equations, so that faster and acceptable solutions can be obtained.

1. Introduction

Sudden change of the flow rate through a hydraulic turbine may trigger considerable change in pressure in the penstock and the headrace tunnel of a hydropower plant, which is typically damped using facilities like surge tanks. Appropriate shapes and dimensions of surge tanks are decisive for their proper functioning, so that reasonable attention is paid to this during the design and construction of hydropower plants. Modernization or refurbishment of existing hydropower plants may however lead to mismatch of optimum conditions for the existing surge tank structure and the operating conditions of the newly installed machinery, requiring thus certain structural modifications in order to allow maximum exploitation and efficiency of the power plant.

A method for analysis of water behavior in surge tanks is studied. Water elevation is adopted as decisive criterion for assessment of functioning of an existing surge tank exposed to increased flow rates, as expected in the full-load conditions after the modernisation. Numerical calculations of the water flow and the free-surface motion based on the computational fluid dynamics (CFD) approach are conducted. Attention is paid to treatment of the inlet boundary condition. The numerical results are compared both with analytical solution and with the experimental data obtained in the real-scale testing on an existing hydropower plant.

2. Problem description

After the modernization of the Hydropower Plant Jablanica, Bosnia-Herzegovina, the installed power of the 6 Francis turbines is increased from 150 MW to 180 MW, which assumes increase in flow rate at full load from 30 m^3/s to 34.5 m^3/s per turbine, or from 90 m^3/s to 103.5 m^3/s per headrace tunnel (there are two headrace tunnels and penstocks, supplying the water to three turbines each). However, in the case of sudden flow rate changes, such a high flow rate might trigger disturbances in functioning or even damage of the surge

* *Corresponding author:* University of Sarajevo - Mechanical Engineering Faculty
Vilsonovo šetalište 9, 71000 Sarajevo, Bosnia-Herzegovina; torlak@mef.unsa.ba

tank and the equipment. Specifically, the closure process leads to free-surface elevation which might cause serious damage of the equipment when it exceeds the tolerated level – upper side of the water chamber on the left-hand side, see Fig. 1 where the surge tank of HPP Jablanica is shown. Hence, correct prediction of the free-surface behavior at load rejection is essential and allows proper assessment of the surge tank operation.

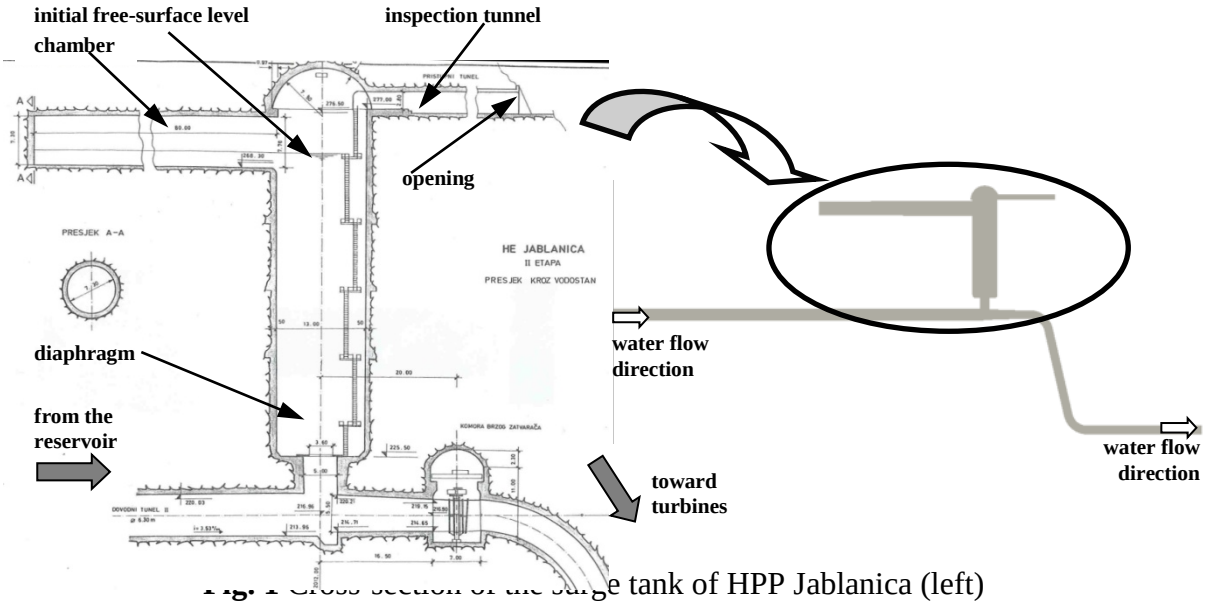

Fig. 1 Cross section of the surge tank of HPP Jablanica (left) and its geometric model as used in simulation (right).

The length of the headrace tunnel between the water intake and the surge tank is 1950 m, the total decline ammounts to about 5 m. Its inner diameter is 6.3 m. The axis of the headrace tunnel beneath the surge tank is positioned 217 m a. s. l. The junction between the tunnel and the tank has diameter of 5 m, with a diaphragm for additional damping whose inner size is 3.6 m. The inner diameter of the surge tank is 13 m, and its maximum height is 66.5 m measured from the axis of the headrace tunnel. The water chamber is 80 m long, and its diameter reduces from 7.70 m to 7.30 m. It is positioned 55 m above the headrace tunnel centerline.

3. Analytical solution

There is a variety of analytical formulations to describe the behaviour of the water surface in a surge tank. They are usually obtained from differential equations governing the conservation of mass and linear momentum.

Here, the simple expressions from literature, obtained assuming cylindrical shape of the surge tank mounted above the horizontal pipeline and neglecting wall friction and other damping effects such as shape-triggered pressure drops, are shown respectively for water elevation in time, maximum water elevation (amplitude) and the period of water oscillations in the tank:

$$z(t) = z_{\max} \sin \sqrt{\frac{g}{L}\frac{A_t}{A_{st}}}\, t \ , \ z_{\max} = \frac{Q_t}{A_{st}} \sqrt{\frac{L}{g}\frac{A_{st}}{A_t}} \ , \ T = 2\pi \sqrt{\frac{L}{g}\frac{A_{st}}{A_t}} \ . \tag{1}$$

z is the vertical displacement of the free-surface in the tank, L is the length of the headrace tunnel, A_t is the cross-section area of the tunnel, A_{st} is the cross-section area of the tank, t is the time, g is the gravity acceleration, Q_t is the flow rate through the tunnel, T is the period of

the water oscillations in the surge tank.

In the case of the surge tank with a chamber, a simple correction of eq. (1) is employed by modifying the cross-section area A_{st} so that the volume of the assumed cylindrical tank is equal to the total volume of the surge tank with the chamber.

Emanating from the geometric data of the example surge tank considered, the oscillation period for the simple cylindrical tank would be about 182.7 s, and the corrected value accounting for the side chamber is about 225 s. The amplitude of the free-surface elevation for the current design flow rate of 90 m^3/s is about 15 m, which is unrealistically high.

4. Computational Fluid Dynamics (CFD)

Two-phase flow of water and air in the surge tank is regarded as flow of immiscible phases with sufficiently sharp interface – free surface of the liquid. It is calculated using a volume-of-fluid approach with interface capturing [1, 2].

Flow of an effective fluid mixture is observed in a control volume under consideration, assuming that the both phases share the velocity and the pressure. The properties of the effective fluid mixture, density and viscosity, are the volume-averaged properties of the individual phases. While the effective fluid motion is described by the Navier-Stokes equations given here in integral form:

$$\frac{\partial}{\partial t}\int_V \rho \,\mathrm{d}V + \oint_S \rho \vec{v}\,\mathrm{d}\vec{S} = 0\,, \tag{2}$$

$$\frac{\partial}{\partial t}\int_V \rho \vec{v}\,\mathrm{d}V + \oint_S \rho \vec{v} \otimes \vec{v}\,\mathrm{d}\vec{S} = -\oint_S p\,\mathrm{d}\vec{S} + \oint_S \mu\left(\nabla\vec{v} + \nabla^{\mathrm{T}}\vec{v}\right)\mathrm{d}\vec{S} + \int_V \rho\, \vec{f}_{\mathrm{b}}\,\mathrm{d}V\,, \tag{3}$$

the behavior of the transported phase (typically, the liquid phase) is described by the scalar transport equation for the phase volume fraction c:

$$\frac{\partial}{\partial t}\int_V c\,\mathrm{d}V + \oint_S c\vec{v}\,\mathrm{d}\vec{S} = 0\,. \tag{4}$$

In eqs. (2-4), the flow properties represent local, instantaneous values, where $\vec{v}$ is the velocity vector, p is the pressure, ρ is the density, μ is the dynamic viscosity, $\vec{S}$ is the control surface, V is the volume within the control surface, t is the time, and $\vec{f}_V$ is the vector of body forces accounting for gravity effects.

The sources or sinks of the phases in eqs. (2) and (4) are neglected, since they are not relevant for the problem considered here. Both water and air are regarded as incompressible, hence density ρ is assumed to be constant across the control volume and in time, and may be omitted from eq. (2).

Turbulence effects which may arise particularly in the region occupied by the air are described by two additional transport equations for the turbulent kinetic energy and the specific dissipation rate according to the k-ε turbulence model [3].

The solution domain is represented by an unstructured set of contiguous, non-overlapping boundary-fitted cells bounded by an arbitrary number of flat faces. Eqs. (2-4) and turbulent transport equations are applied to each cell and discretized using a finite-volume method [3, 4]. The collocated arrangement with all solution variables referring to the cell centroids is

employed. The surface and volume integrals are approximated using the midpoint rule. A linear-upwind scheme, which is formally second-order accurate, is used for discretization of the convective terms, while high-resolution interface capturing scheme (HRIC) [1, 2] is used in eq. (4). The face contributions from the viscous/diffusion term are obtained by differencing the variable values from the neighbor cell centroids, and include a correction term in order to suppress possible oscillations caused by grid non-orthogonality [4]. The gradients are calculated by blending the Gauss method and the weighted least-square method, with the blending factor depending on the grid quality and appropriate limiting taking into account the variable values from the neighbor cells.

The considered time interval is subdivided into a finite number of the time steps of the same size, and an implicit time integration scheme is applied to promote stability [3]. The resulting systems of equations assembled for each solution variable are processed sequentially in turn. They are solved employing an algebraic multigrid method.

All calculations are performed using the CFD software *STAR-CCM+* [5].

5. Computational model

The geometric model includes the headrace tunnel, the surge tank with the diaphragm, chamber and the inspection tunnel, as well as the penstock, see Fig. 2. The length of the headrace tunnel in the model has significant effects on the static pressure and water elevation variation, hence the complete tunnel is taken into account. Due to symmetric shape of the geometric model, symmetric flow behavior is expected. Hence, only a half of the model is considered in the calculation, applying the appropriate symmetry condition as the boundary condition in the midplane.

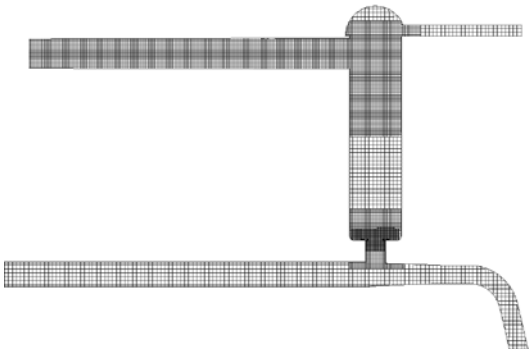

Fig. 2 Computational grid in a part of the solution domain. Local grid refinement in the diaphragm region and in the region of expected free surface motion is seen.

The computational grid contains about 80.000 cells, which are trimmed at the boundaries, while the rest of them is of cubical shape yielding the optimum grid quality at the shared interior cell faces. The grid is locally refined in the diaphragm region as well as in the free-surface region, where strong flow variations are expected. The time step size used is of order of magnitude of 0.1 s, to keep the Courant-number values in the vicinity of the free-surface sufficiently low. These time steps sizes are sufficiently fine with respect to the expected oscillation periods (~200 s) so that even 1st-order implicit Euler scheme provides acceptable results. The total simulated time is between 300 s and 600 s, which depends on the operating conditions simulated.

The boundary condition at the turbine side of the penstock (wicket-gate closure) is specified as linear variation of the flow rate, from the operating level $Q_{t,n}$ to zero, within the prescribed closure time between the instant of the closure start t_1 and the instant of the closure end t_2:

$$Q_{\mathrm{t}}(t)=\begin{cases} Q_{\mathrm{t,n}}, & t<t_1 \\ Q_{\mathrm{t,n}}\dfrac{t_2-t}{t_2-t_1}, & t_1\le t\le t_2 \\ 0, & t_2<t \end{cases}. \tag{5}$$

At the opening of the inspection tunnel (upper-right boundary), static, atmospheric pressure condition is specified.

Numerical tests have shown that simulation results strongly depend on the inlet boundary condition while commonly used types of are employed all the time of simulation. Constant incoming flow rate is not applicable, since this would lead to the constant filling of the surge tank after the turbine closure which is not the case in reality. On the other hand, if initialization of the flow field is inadequate, pressure specification at the inlet exhibits rather unstable behaviour prior to the turbine closure, enforcing unrealistically large amounts of water to flow from the surge tank into the penstock. Hence, in order to provide proper initial flow in the tunnel and the penstock, the constant flow rate is specificed at the inlet boundary for a relatively short interval of time before the turbine closing starts (typically 1-2 s). After this, the stagnation condition – the total pressure far upstream, where the fluid is assumed to be at rest: $p_{\mathrm{tot}}=\rho_{\mathrm{water}}\,g\left(z_{\mathrm{ref}}-z\right)$ with z_{ref} being the elevation of the free surface in the reservoir, and z the vertical position of the boundary point – is employed relating the static pressure and the velocity magnitude at the inlet via Bernoulli's equation.

6. Results

In Fig. 3, CFD prediction of the water phase distribution at a number of typical time steps, with non-equal time difference between the individual steps, is shown. The arrows depict main flow direction. A comparison of the CFD results with the photographs from the real-scale test for the same operating conditions, shown in Fig. 4, reveals certain agreement indicating that the most typical motion patterns are captured by the simulation: water rising in the tank, water entrance into the side chamber, reflection from the side chamber wall with back flow from the side chamber, and simultaneous back flow from the chamber and water sinking in the tank.

More detailed comparison is given in Fig. 5 where the time histories of the maxmimum water elevation in the tank for two different cases, for which the real-scale testing data exist, are shown. Analytical solutions from eq. (1) are shown as well. The blue dotted line indicates approximately the position of the lowest point, while the red dashed line indicates the position of the highest point of the water side chamber (the latter represents approximately the limit of the free surface position tolerance).

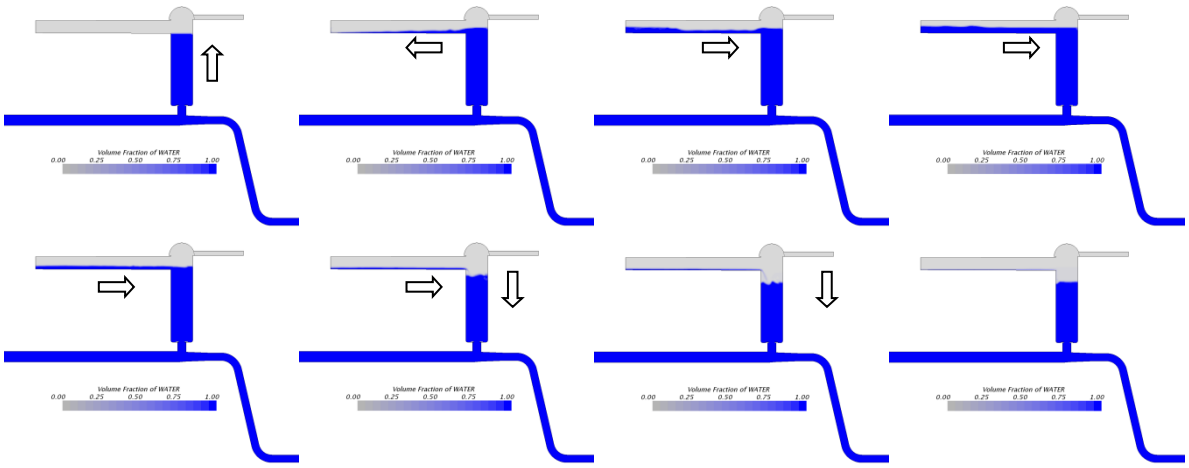

Fig. 3 A sequence of the water phase distribution (blue) at a number of different time steps, illustrating free surface motion in the surge tank.

(a) (b) (c)

(d)

Fig. 4 Observations from the real-scale testing: water rising in the tank (a), water flow into the side chamber (b), back flow from the side chamber (c), simultaneous back flow from the chamber and water sinking in the tank (d).

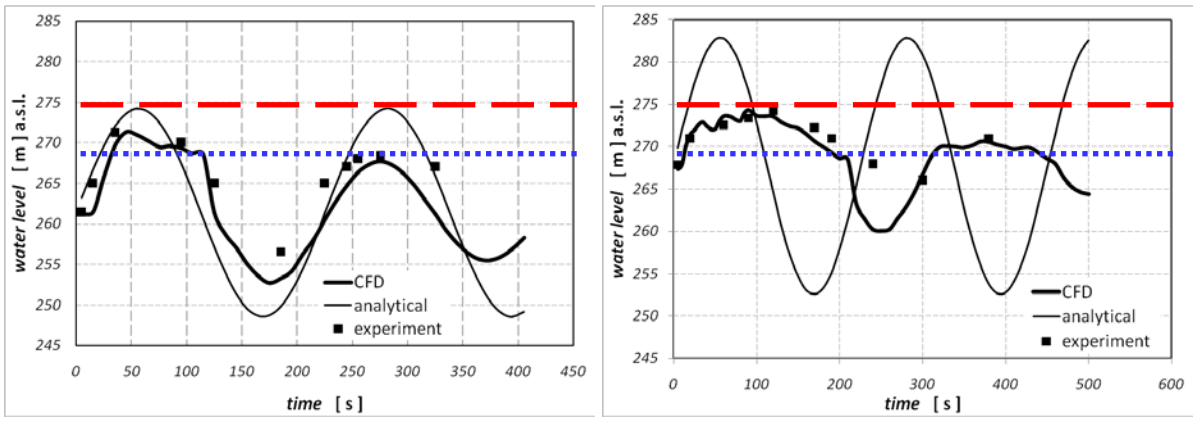

Fig. 5 Time history of the maximum water elevation in the surge tank for two different operating conditions: Q_t =72 m^3/s and initial water level 261.4 m a.s.l. (left), and Q_t = 84.8 m^3/s and initial water level 267.9 m a.s.l. (right).

For assessment of the surge tank functioning the first oscillation period is relevant, since that is when the highest amplitude arises.

In the case with the lower flow rate and the lower initial water level (Q_t =72 m^3/s, z_0=261.4 m, Fig. 5 left), the free surface rises until it reaches the side chamber, and subsequently enters it, keeping roughly the same surface level for about 90 s (reflection and back flow from the side chamber), which is still below the tolerance limit (red dashed line). CFD results agree well with the measurement findings, and reproduce the reflection and back-flow effect. The

analytical solution of the water oscillation period agrees realtively well in the first oscillation, however the amplitude of the water surface motion reaches the tolerance limit, which means that the functioning of the surge tank at these operating conditions would be questionable.

Fig. 5 right shows the case with the higher flow rate Q_t = 84.8 m^3/s (slightly lower than the current design flow rate) and the higher initial water level z_0=267.94 m (corresponds to the design head of the plant), where the tolerance level of the free surface position is almost reached. The oscillation period is noticeably longer. CFD simulation reproduces these effects as well. Analytical solution, since no damping included, exhibits the same oscillation period as in the previous case, while the oscillation amplitudes are much higher and considerably beyond the tolerance limit.

7. Conclusions

CFD analysis of the water flow in a surge tank provides detailed information on the flow phenomena in the surge tank enabling their thorough understanding. Agreement between the simulation results and the experiment is acceptable, enhancing reliability of the surge-tank operation assessment. The computational costs are much higher as compared to analytical solution or numerical solution of the simplified surge-tank models based on mass and linear-momentum conservation equations.

Further investigation will be focused on the analysis of friction losses and the pressure losses in the tank and the diaphragm, attempting to improve the analytical solution or simplified surge-tank model equations which should allow faster calculation with acceptable accuracy.

References

[1] Muzaferija S., Perić M.: „Computation of free surface flows using interface-tracking and interface-capturing methods". In: *Nonlinear water wave interaction*, Chap. 3, Eds. O. Mahrenholtz, M. Markiewicz, Computational Mechanics Publications, Southampton, 1998.

[2] Muzaferija S., Perić M., Sames P., Schelin T.: „A two-fluid Navier-Stokes solver to simulate water entry". *Proc. Twenty-Second Symposium on Naval Hydrodynamics*, 1998.

[3] Ferziger J.H., Perić M.: „*Computational Methods for Fluid Dynamics*". Springer, 2013.

[4] Demirdžić I., Muzaferija S.: „Numerical Method for Coupled Fluid Flow, Heat Transfer and Stress Analysis Using Unstructured Moving Meshes with Cells of Arbitrary Topology". *Comput. Meth. Appl. Mech. Engrg.*, 125, pp. 235-255, 1995.

[5] CD-adapco: „*User Guide, STAR-CCM+ Version 9.04*". www.cd-adapco.com, 2014.